



Full Length Article



Scale-up study of electrochemical carbon dioxide reduction process through data-driven modelling

Guyu Zhang^a, Xiaoteng Liu^{a,b,*}, Hanhui Lei^{b,*}, Yucheng Wang^c, Denise Bildan^b, Xiangqun Zhuge^a, Lei Xing^d, Kun Luo^{a,*}

^a Changzhou Key Laboratory of Intelligent Manufacturing and Advanced Technology for Power Battery, School of Materials Science & Engineering, Changzhou University, Changzhou 213164, PR China

^b Department of Mechanical and Construction Engineering, Faculty of Engineering and Environment, Northumbria University, Newcastle upon Tyne NE1 8ST, U.K

^c Cardiff Catalysis Institute, School of Chemistry, Cardiff University, Cardiff CF10 3AT, United Kingdom

^d School of Chemistry and Chemical Engineering, University of Surrey, GU2 7XH, United Kingdom

ARTICLE INFO

Keywords:

Scale-up
Electrochemical
CO₂ reduction
Mass transfer
Machine learning

ABSTRACT

Efficient electrochemical carbon dioxide reduction (eCO₂RR) depends on addressing mass transfer kinetics hindering CO₂ diffusion to the cathode surface. Gas diffusion electrodes (GDE) have enhanced this process, but the shift from lab-scale research to industrial use is to be explored, and we systematically assessed four variable factors: electrode area, gas flow rate, catalytic layer (CL) thickness and gas diffusion layer (GDL) porosity for scaling-up the electrolyser with a comprehensive two-dimensional physical model was developed to investigate the concentration, distribution, and consumption of CO₂. Random Forest (RF) coupled with Latin Hypercube Sampling (LHS) data collection method demonstrate a prediction accuracy of 98.67 % and a RMSE of 0.00058 for the average CO₂ concentration. A maximum CO₂ consumption rate of 98 % was achieved at a CL thickness of 73 μm and a GDL with a porosity of 0.8, for an electrode area of 100 cm² and a gas flow rate of 91 mL/min. This high level of CO₂ consumption was sustained throughout the scaling-up process, consistently at 96.7 %, as the evidence attests to the reliability and feasibility of the scale-up approach.

1. Introduction

The process of capturing carbon dioxide (CO₂) followed by electrochemical conversion has attracted increasing attention in research circles due to its numerous advantages, which include operating at a moderate reaction temperature, utilising a simple reaction setup, and yielding high-energy-density fuel products like carbon monoxide (CO) and formate etc [1–4]. This method stands out as one of the most efficient approaches for large-scale energy storage, chemical production, and transportation systems. Furthermore, eCO₂RR represents a highly controllable process, enabling the generation of various products by adjusting factors such as catalyst structure, electrolyte pH, applied potential, and electrolyser design [5–9]. However, the inherent inertness of CO₂ molecules necessitates a high activation potential, and the limited solubility of CO₂ in the electrolyte (approximately 35 mM at 298 K, 1 atm) can impede CO₂ mass transfer, potentially leading to the competing hydrogen evolution reaction (HER) at the cathode side [10–12].

GDE reactors are reported to benefit the CO₂ mass transfer, which allows CO₂ fed directly through the GDL to the catalyst active sites in a short diffusion distance [13–15]. Diffusion in GDL has been reported by Wang et al. [16], who developed a hybrid eCO₂RR reactor using bilayer porous electrode. By the directional diffusion of gas molecules onto the CL, 94 % Faraday Efficiency (FE) to carbonaceous products at –1.0 V vs. RHE and a current density of 200 mA cm⁻² was achieved. Albo et al. [17] evaluated the effect of current density, electrolyte flow rate/area ratio and CO₂ gas flow rate/area ratio on a GDE reactor and realised that the reactor was able to catalyse CO₂ reduction for more than 20 h. A well designed porous/hydrophobicity of CL is reported to benefit the microenvironment near the electrode site and promote the CO₂ mass transfer. Xing et al. [18] demonstrated a PTFE treated hydrophobic CL supported on carbon paper as GDE. This configuration led to enhanced reaction activity and FE, achieving a partial current density to 250 mA cm⁻² and single-pass conversion rate of 14 % at moderate potentials, achieved through the precise control of the hydrophobicity of electrode

* Corresponding authors at: Changzhou Key Laboratory of Intelligent Manufacturing and Advanced Technology for Power Battery, School of Materials Science & Engineering, Changzhou University, Changzhou 213164, PR China (X. Liu).

E-mail addresses: terence.liu@northumbria.ac.uk (X. Liu), hanhui.lei@northumbria.ac.uk (H. Lei), luokun@cczu.edu.cn (K. Luo).

<https://doi.org/10.1016/j.fuel.2024.132400>

Received 6 March 2024; Received in revised form 28 June 2024; Accepted 2 July 2024

Available online 3 July 2024

0016-2361/© 2024 The Author(s). Published by Elsevier Ltd. This is an open access article under the CC BY license (<http://creativecommons.org/licenses/by/4.0/>).

surface. Wang et al. [19] developed a Cu₂O/Graphene electrocatalyst, where the presence of the 2D graphene and 3D Cu₂O nano flower enables a microporous scaffolding structured CL. The pores which benefit the CO₂ mass transfer and effectively improve the activity and efficiency of eCO₂RR. However, such reported works confined to the laboratory scale, which is far from reaching industrial viability. In contrast to fundamental research, the large-scale integration of CO₂RR technology remains in its nascent stages, necessitating the development of large-scale CO₂ electrolyzers.

Scaling-up of the reactor includes issues related to the distribution of reactant gases and the imperative need to ensure uniform gas distribution across the CL. This uniformity is essential to prevent any distinct areas of the catalyst from being fully exposed to the electrolyte. Additionally, the mechanical properties of the GDL, particularly its strength in tolerating gas pressure at a large scale. It is well known that selectivity, activity and stability are key parameters that hinder the industrial implementation of electrochemical CO₂ reduction. Each of these parameters has been investigated by focusing on the nature of the electrocatalysis, the morphology of the electrocatalyst, the electrolyte composition and the process conditions [20–22]. While ongoing research on scale-up includes various economic assessments in plant settings, there remains a scarcity of practical demonstrations at this scale. Moreover, establishing long-term stability is an essential requirement for the viable operation of commercial processes. Seonhwa Oh et al. [23] developed a large-area gas diffusion electrode (25.5 and 136 cm²) with high conversion efficiency and high cell performance, and further applied it to a CO₂ electrolyser with an effective area of 107.44 cm², which resulted in CO conversion efficiencies ranging from 41.99 %–57.75 % at 2.2–2.6 V. The performance of GDE depends strongly on the local environment within the CL and the balance between transfer phenomena and reaction kinetics. Based on the reported higher partial pressures and concentrations of CO₂ to saturate the FE of CO, Li et al. [24] found that flow rates from 1 to 50 mL/min resulted in increasing current densities in the overall geometry, which saturated at high flow rates. Lei et al. [25] investigated the single variation and interaction of Pt loading in the CL and the porosity of the GDL, and the fact that Pt distribution presenting inhomogeneity improves the current confinement, and the porosity of the GDL also exerts a great influence on the battery performance. Gao et al. [26] investigated the effect of porosity and thickness of the GDL on the effective diffusion coefficient, and the results showed that the effect of pore size on the transport properties was greater than that of thickness, especially in the direction of the penetration surface, and the thickness had almost no effect on the permeability. Similar to the fluid saturation values, the flux values change drastically as the porosity increases from 0.6 to 0.7, 0.8 and 0.9. The results also demonstrate that the flux changes are more drastic at higher porosities, which is natural since both porosity and saturation affect the effective diffusion coefficient.

One of the challenges hindering the scaling-up of eCO₂RR electrolyzers is the inadequate and non-uniform distribution of CO₂ molecules on the catalyst surface. This phenomenon results in reduced CO₂ utilization, low and uneven current density, and compromised FE [27,28]. To enhance selectivity for CO₂ reduction while inhibiting hydrogen generation, a significant competing reaction occurs at the cathode-electrolyte interface. This reaction is influenced by various factors, including solution pH, electrolyte composition, temperature, pressure, potential, CO₂ concentration, as well as the chemical and morphological attributes of the catalyst [29]. All these factors require careful consideration. Researchers conducted numerous experiments to determine optimised manufacturing options, but the substantial investment of time and resources has severely limited the feasibility. Furthermore, complex experiments encompass a multitude of variables, potentially leading to testing standard ambiguities.

Designing highly accurate physical models for multiple types of electrolyzers and operating environments is a very difficult task [30]. Solving this bottleneck is possible thanks to the rapid development of

artificial intelligence (AI) technology. AI algorithms can extract useful information from raw data and output independent decisions when performing industrial tasks.

The development of models that can perform precise simulation for electrolyser still remain a challenge. However, addressing this bottleneck has become achievable due to the swift progression of AI technology. AI algorithms possess the capability to discern valuable insights from unprocessed data and autonomously make informed decisions while executing industrial tasks. The main commonly used ML algorithms are Recurrent Neural Network (RNN), Support Vector Machine (SVM), and RF [31–33]. Algorithms are evaluated on the basis of accuracy. Zheng et al. [34] investigated the polarisation curve prediction and performance degradation prediction of Proton Exchange Membrane Fuel Cells (PEMFC) using Long Short-Term Memory (LSTM). The coefficients of determination (R²) of the LSTM models with different training data were greater than 0.95. Han et al. [35] conducted a study comparing the performance of PEMFC using Artificial Neural Networks (ANN) and SVM algorithms. They considered input variables such as temperature, humidity, and pressure. The results demonstrated that the ANN model achieved outstanding predictive accuracy, with a high score of 0.9995, outperforming the SVM model with a predictive accuracy of 0.982. Huo et al. [36] have proposed a predictive method that combines the RF algorithm with the Convolutional Neural Network (CNN) model. Additionally, advanced deep learning techniques, such as batch normalization and dropout layers, have been employed to enhance the model's generalization capability. The research findings indicate that, in the majority of cases, this predictive model consistently achieves an accuracy rate exceeding 90 %. The predictive curve of this model closely aligns with the actual curve. Consequently, this model has the potential to significantly reduce experimental time and costs. All of the above-mentioned algorithms can be adopted for in electrolysis reactor research and design. However, in real-world cases, the specific data characteristics, problem types and requirements will be the decisive factors that lead to the high or low accuracy of AI algorithms.

Several issues persist when employing these single-variable multi-parameters, including: Notably, not all single parameters exhibited significant changes in the scaled-up studies; Simultaneous studies of multi-parameter interactions were overlooked due to the single-variable principle's application; The consideration of simultaneous changes in both directions was omitted for each single direction; Additionally, the simulation process is characterized by its time-consuming nature and its dependence on computational resources.

The aim of this study is to reveal the effect of variations in GDL porosity, electrode area, CL thickness, and the gradient of gas volumetric flow rate on CO₂ concentration throughout the scaling-up process. When increasing the electrode area from 1 cm² to 100 cm², there is a significant decrease in CO₂ concentration, dropping from 30.92 mol/m³ to 0.99 mol/m³. Similarly, when the CL thickness is increased from 5 μm to 55 μm, CO₂ concentration also decreases from 13.65 mol/m³ to 6.92 mol/m³. Simultaneously, the porosity of the GDL and the gas volumetric flow rate influence CO₂ concentration, although the change in concentration is relatively small, around 1 mol/m³. By utilizing ML algorithms and employing various analytical techniques, we conducted a comprehensive investigation. Remarkably, even as we scaled up the process, we managed to pinpoint the specific conditions necessary to sustain a robust CO₂ consumption rate of 96.7 %, mirroring the outcomes observed at the laboratory scale. Furthermore, our study sheds light on the development of a cost-effective industrial engineering design methodology, leading to reduced labour expenses and providing precise details on high-performance electrolyser manufacturing.

2. Model development and validation

A two-dimensional model was developed, consisting of four parts: gas chamber (GC), GDL, CL and the electrolyte channel (ELEC), as shown in Fig. 1. They are rectangular compartments arranged in parallel, with

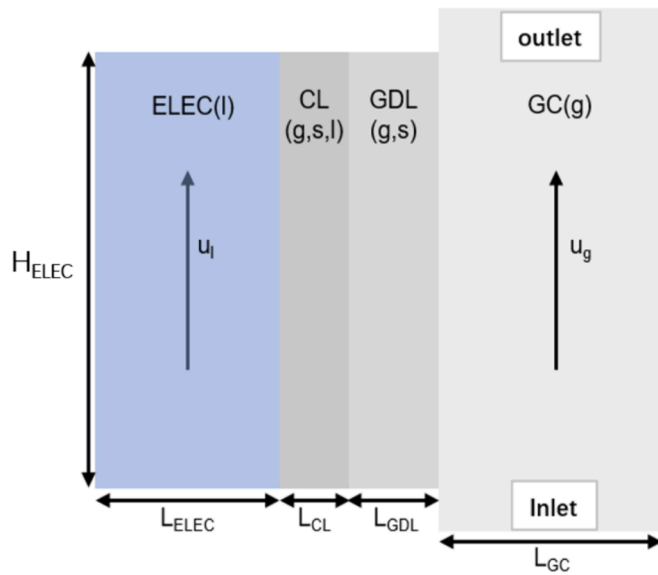


Fig. 1. Two-dimensional cathode-side CO₂ reduction electrolyser.

the same height and width but varying thicknesses. The feed gas enters the system from the bottom of the GC and exits along with other gaseous products such as CO and H₂ on the opposite side. A current collector is placed between the GC and the GDL. Its main function is to supply electrons, with negligible ohmic loss compared to the GDL and the CL. CO₂ and electrons are transported via diffusion and conduction respectively through the porous hydrophobic GDL and react in the CL. It is widely recognized that only dissolved CO₂(aq) serves as the active reactant for electrochemical reactions, rather than HCO₃⁻, CO₃²⁻, or CO₂(g). Therefore, gas-liquid mass transfer for CO₂(aq) in the CL should be taken into account. The CL consists of a layer coated with granular Cu_xO catalyst (a mixture of Cu₂O, CuO, and Cu), offering a non-toxic and abundant option suitable for scaling up and holding promise for generating multi-carbon products. The electrolyte (potassium hydroxide, KOH) and the aqueous products (i.e. formate) flow through the ELEC.

2.1. Model assumptions and characteristics

The multiphysics field model is based on the following assumptions:

- (1) The variation of the flow rate is fixed in the range of $Ma < 0.3$, consistent with laminar flow conditions, it is maintained at a low flow rate with a Reynolds number of about 10^{-2} [37]. Thus the reacting gases passing through the cathode channel are considered to be laminar.
- (2) Constant flow rates and a uniform supply of gas can help maintain flow stability in the system, and the flow path is straight from bottom to top to avoid instability and eddies in the flow. An adequate supply of CO₂ is uniformly supplied at the cathode inlet at a constant flow rate, and the ideal gas law is applied to the gas species.
- (3) It is assumed that gas mass transfer occurs only through diffusion and convection mechanisms. The relatively weak interaction between the gases in a system with a low density and low flow rate allows the drag effect on the overall gas flow to be simplified or ignored.
- (4) A reasonable isothermal assumption was used because the presence of a flowing liquid (a good conductor of heat) electrolyte in the model would carry away the heat generated by the relatively

low current density of about 102 mA/cm². The Soret effect of mass transfer is therefore not considered.

- (5) The pH of the anode body solution is kept constant, and no acid-base equilibrium occurs at the catalyst layer-electrolyte boundary.
- (6) The model investigates the CO₂ mass transfer process on the cathode side, where the gas flow rate is less than 100 mL/min and the resulting pressure is not sufficient to break through the membrane.

The model processes: 1) conservation of mass, matter, charge, and momentum; 2) migration of matter through the porous electrodes by diffusion and convection mechanisms; and 3) generation and consumption of species within the CL powered by electrical energy. In addition, the physical properties of the CL, such as thickness, pore size and porosity, were modelled.

2.2. Governing equation

2.2.1. Gaseous substance

There are four distinct gaseous components: CO₂, N₂, H₂, and CO. At the inlet, a gas mixture consisting primarily of CO₂ with a mass fraction of 0.999 is introduced, with the remaining gases being N₂. CO is one of the byproducts of reduction reactions, whereas H₂ is produced because of the water electrolysis reaction. These gaseous components are distributed across three regions: the CL, the GDL, and the GC. To maintain mass conservation, we employ Eq. (1) as a modelling basis with assumption of a constant temperature and do not account for the Soret effect in the diffusion. The subscript *i* in the formula denotes the corresponding different species of gas substances [38].

$$\nabla \cdot (-\rho_g D_{i,m} \nabla \omega_i - \rho_g \omega_i D_{i,m} \frac{\nabla M_g}{M_g}) + \nabla \cdot (\rho_g u_g \omega_i) = R_{i,m} \quad (1)$$

$$M_g = \left(\sum_i \frac{\omega_i}{M_i} \right)^{-1} \quad (2)$$

ρ_g is the average density of multiple gases when they are mixed; ω_i is the mass fraction for gas; M_g is the average molar mass of the gas mixture calculated as shown in Eq. (2); M_i is the molar mass of gas; $D_{i,m}$ is the diffusion coefficients of the gas *i* in the medium *m*; and u_g is the velocity of the gas mixture. It is important to note that the $R_{i,m}$ term has a zero value in both the GC and GDL.

2.2.2. Liquid type

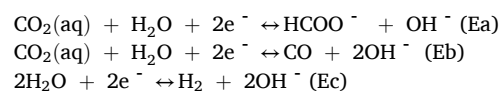
The conservation of mass of the water-bearing material *j* is modelled by the Nernst-Planck Eq. (3) [33].

$$\nabla \cdot (-\rho_l D_{j,m} \nabla \omega_j - \frac{z_j F \rho_l \omega_j D_{j,m} \nabla V_l}{R_{ideal} T} + \rho_l \omega_j u_l) = R_{j,m} \quad (3)$$

where ρ_l is the density of the liquid mixture; z_j is the valence electrons of the ionic species; R_{ideal} is the ideal gas constant; T is the operating temperature; u_l is the liquid flow rate, and q_l/A_{ELEC} is the ratio of volumetric flow rate to the cross-sectional area of the liquid chromatogram; $D_{j,m}$ is the diffusion coefficient of the aqueous substance, which can also be corrected by the Bruggeman's relational equation in porous media.

2.2.3. Gas-liquid mass transfer

In this scenario, two competing electrochemical reduction reactions of CO₂ occur in the electrolyte [33].



For gas–liquid transfer in the CL, we focus solely on the CO₂ transfer due to the negligible solubility of CO and H₂. Therefore, the rate of gas–liquid transfer rate for CO₂ is [33].

$$R_{p,CO_2}(aq) = -R_{p,CO_2(g)} = a_{gl}K_{GL}M_{CO_2}\left(\frac{P_{CO_2(g)}}{H_{CO_2}} - C_{CO_2(aq)}\right) \quad (4)$$

where a_{gl} is the gas–liquid specific interfacial area; K_{GL} is the total mass transfer coefficient; H_{CO_2} is the Henry's constant of CO₂, which factors in the salting out effect; $P_{CO_2(g)}$ is the partial pressure of CO_{2(g)}, which is calculated according to Dalton's law; $P_{CO_2(g)} = P_{CL} \times CO_{2(g)}$; and $C_{CO_2(aq)}$ is the concentration of dissolved CO₂ in the electrolyte [33].

$$a_{gl} = 2 \frac{\epsilon_{CL}^0 (r_{p,CL} - \delta_{ele})}{r_{p,CL}^2} \quad (5)$$

2.2.4. Electrode kinetics

The current densities which corresponds to the reactions (Ea) to (Ec), i_{Ea} , i_{Eb} and i_{Ec} were determined using Tafel dynamics [33].

$$i_{Ea} = -i_{o,Ea}^{ref} \left(\frac{C_{CO_2}(aq)}{C_{CO_2(aq),Ea}^{ref}} \right) \exp\left(-\frac{\beta_{Ea}F}{R_{ideal}T} (V_s - V_1 - V_{eq,Ea}^{ref})\right) \quad (6)$$

$$i_{Eb} = -i_{o,Eb}^{ref} \left(\frac{C_{CO_2}(aq)}{C_{CO_2(aq),Eb}^{ref}} \right) \exp\left(-\frac{\beta_{Eb}F}{R_{ideal}T} (V_s - V_1 - V_{eq,Eb}^{ref})\right) \quad (7)$$

$$i_{Ec} = -i_{o,Ec}^{ref} \exp\left(-\frac{\beta_{Ec}F}{R_{ideal}T} (V_s - V_1 - V_{eq,Ec}^{ref})\right) \quad (8)$$

where $i_{ref\ o,Ea}$, $i_{ref\ o,Eb}$ and $i_{ref\ o,Ec}$ are the exchange current densities for each catalyst surface area under reference conditions; $C_{ref\ CO_2(aq),Ea}$, $C_{ref\ CO_2(aq),Eb}$ are the reference concentrations of CO_{2(aq)} corresponding to the reaction (Ea) and the reaction (Eb), respectively; β_{Ea} , β_{Eb} , and β_{Ec} denote the symmetry factors

associated with the formation of HCOO⁻, CO and H₂, respectively; F is the Faraday constant; $V_{ref\ eq,Ea}$, $V_{ref\ eq,Eb}$ and $V_{ref\ eq,Ec}$ are the equilibrium potentials for the reactions (Ea) to (Ec) at the reference conditions and operating temperatures, respectively.

The local electron and electrolyte potentials V_s and V_1 are derived from Ohm's law and the principle of charge conservation [33].

$$\nabla \cdot (-\sigma_{s,m}^{eff} \nabla V_s) = Q_{s,m} \quad (9)$$

$$\nabla \cdot (-\sigma_{l,m}^{eff} \nabla V_1) = Q_{l,m} \quad (10)$$

where $\sigma_{s,m}^{eff}$ and $\sigma_{l,m}^{eff}$ are the effective conductivities of the solid material and electrolyte. These values are constants and are corrected for $(1 - \epsilon_m)$ and $\epsilon_m S_m$ according to the Bruggeman equation in porous media, with $Q_{s,m}$ and $Q_{l,m}$ as source terms; respectively. Other control equations Ref. SI(1–13).

2.3. Boundary condition

The gaseous species in the GC, GDL, and CL are collectively modeled. At the inlet of the GC, the mixture gas composition and velocity are set to be identical to those of the inlet mixture gas. Ambient pressure (i.e., 1 atm) is assumed for the outlet mixture gas at the GC outlet, with non-diffusive species. Zero-flux for gaseous species is applied at the ELEC/CL interface, assuming that any gas can only escape from the GC. Pressure remains continuous at the GDL/GC interface.

2.4. Numerical calculation method

Above equations were developed using COMSOL Multiphysics 5.6, with the volume fraction of the substance defined by the coefficient partial differential equations, the rate of transfer and concentration distribution of the substance defined by the Concentrated Substance

Transfer Module, and Darcy's Law describing the fluid flow, and a free tetrahedral mesh was used to integrate the above three main modules for the overall modelling, which used a steady state solver to facilitate the observation of the CO₂ concentration distribution in the CL under steady-state conditions, which is used to increase the CO₂ concentration in the CL to a relatively saturated value by keeping the intrinsic conditional parameters and adjusting the parameters that are highly affected by local variations.

2.5. AI modelling

In the context of scaling-up modelling research, it is essential to acknowledge that a single variable may not give accurate results. This limitation arises from the fact that a single variable adjustment cannot eliminate all potential confounding factors or distractors. Therefore, in this study, we selected a constrained set of variations encompassing electrode area, gas flow rate, CL thickness, and GDL porosity as the four key input parameters to drive our model. The resulting output parameter of interest was the average CO₂ concentration within the CL. To generate the necessary dataset, we employed the physically grounded mechanistic model of eCO₂R implemented in COMSOL. Subsequently, we applied the Latin Hypercube algorithm to screen and optimise the data points. These curated data points were subsequently utilized to train ML models, including RNN, RF, and SVM, each serving as a distinct approach to model training and analysis. Refer to SI (14–21) for the formulae of the different algorithms.

2.6. Model training and experimental setup

The model was chosen to be arranged using four variables and one outcome. Among them, the electrode area, gas flow rate and CL thickness were scaled up by magnitude orders (1–100 cm², 1–100 mL/min; 1–100 μm), and the porosity of the GDL conformed to the experimental and commercial values of 0.5–0.9. Steps were set to obtain about 8,000 nodes. The LHS method extracted 10 % of the original number of nodes. LHS ensures a uniform positional distribution between the levels of each factor, and the representative experimental results were screened and used to substitute into the AI algorithm. A performance prediction model was developed using PythonCharm. Four metrics are commonly used to evaluate the performance of performance prediction models, namely: 1) RMSE: Root Mean Square Error. 2) R²: Coefficient of Determination. 3) MAE: Mean Absolute Error. 4) MAPE: Mean Absolute Percentage Error. Reference SI (22–25) for calculation of equations.

3. Results and discussion

The simulation results are categorised into two types: single-variable and combined-variable analyses. In the single-variable analysis, one of the following parameters – electrode area, gas flow rate, CL thickness, or GDL porosity – is selected as the variable, while the other parameters remain constant. Detailed parameters, settings, and conditions in the simulations are summarized in Tables S1 and S2, Supporting Information. In contrast, for combined-variable analysis, all four of these parameters are simultaneously varied. In this case, we conduct exhaustive sampling while ensuring that each parameter adheres to its respective conditions and equidistant sampling criteria. This comprehensive approach allows us to assess how different parameters impact the enlargement of the electrode.

3.1. Univariate analysis

The study primarily examines the variation in the average CO₂ concentration within the CL, serving as a pivotal evaluation metric in the electrode enlargement process. A lower average concentration indicates a higher CO₂ consumption. The research delves into the significance of four parameters: electrode area, CL thickness, gas flow rate, and GDL

porosity, concerning CO₂ conversion during the model calculation. The experimental design adheres to the single-variable approach, investigating how various parameters influence the change of CO₂ concentration within the device while ensuring reaction equilibrium is achieved. The gas is introduced into the device from below the GC, as illustrated in Fig. 1. The gas diffuses through the GDL, culminating in the establishment of a localised region with a high concentration of CO₂ at the inlet of the CL-GDL interface. When the electrode area is varied while the other parameters are kept constant, shown as the range of this high-concentration region corresponds to the region marked in red in Fig. S1. Nevertheless, the concentration within this region consistently maintains a higher value, typically within the range of 37–40 mol/m³, displaying a negligible decreasing trend. This phenomenon arises from the continuous supply of gas, which compensates for the consumed gas, a trend that becomes more pronounced when higher gas flow rates are employed. Consequently, when calculating the average CO₂ concentration within the CL, these results become diluted by the additional gas, thereby influencing the assessment of the device's CO₂ consumption capability. To mitigate this error and enhance result accuracy, the CL's thickness was divided evenly into three segments with identical thicknesses at the front end (proximate to the CL-GDL interface), middle section, and rear end (proximate to the CL-EC interface), as illustrated in Fig. S2. In order to provide a more precise representation of the device's gas conversion capability, the foremost segment, which is particularly sensitive to reduction reactions, was selected as the primary focus for investigating the eCO₂RR within the device.

The primary parameter under investigation is the electrode area, which has been systematically evaluated across six gradient groups: 1, 20, 40, 60, 80, and 100 cm². Other key conditions were kept constant, including the CL thickness (20 μm), GDL porosity (0.8), and gas flow rate (15 mL/min) as outlined in Table S1. The alteration in electrode area is visually depicted by the height shift observed during the 2D simulation model (refer to Fig. S1). It's noteworthy that the highest concentration of CO₂ molar occurs at the surface of the CL adjacent to the gas inlet (Fig. S3), which serves as the primary diffusion center for gas transport. Conversely, the lowest CO₂ concentration is observed at the surface of the EC-CL interface, with a concentration of 6.8 mol/m³. This suggests that unreacted CO₂ may potentially dissolve in the liquid phase or obstruct pores on the surface of the EC-CL, hindering the formation of a three-phase interface and impeding the efficiency of the eCO₂RR.

The CO₂ concentration at the front end, held at a consistent height, shows a clear trend: an increase in consumed CO₂ with an enlarged

electrode area, as shown in Fig. 2. This observation is consistent with the findings presented in Fig. S1, reinforcing the idea that a larger electrode area results in a lower CO₂ concentration. However, it's important to note that the lower gas flow rate provides inconclusive evidence regarding the CO₂ consumption capacity of the enlarged electrode area. For further investigation, a gradient variation in gas flow rates was implemented.

To explore the influence of CO₂ flow rate within the cell, gas flow rates were set at 1, 20, 40, 60, 80, and 100 mL/min while maintaining the constant parameters outlined in Table S1.

Increasing the gas flow rate, enhances the concentration of CO₂ within the cell, as shown in Fig. 3. Notably, The high concentration of CO₂ stays more at 9 μm to the left of the CL-GDL interface, while the increase of gas flow rate will increase the CO₂ concentration at the outlet side, so that the gas distribution inside the whole 9 μm-thickness CL tends to be homogeneous, which is able to improve the stability of the reaction inside the catalytic layer. Meanwhile, with the increase of gas flow rate, the concentration distribution of CO₂ at 11 μm on the EC-CL side did not change significantly, and it was reported that the overall activity would no longer have a direct correlation with the CL thickness after increasing the CL thickness to more than 9 μm [39]. Therefore, a robust gas flow rate demands a minimum thickness for the CL. This is because an excessively high gas flow rate may lead to pore blockage, potentially compromising the generation of the phase interface essential for eCO₂RR and favouring the dominance of the standard electrochemical reaction (RHE). As shown in Fig. S4, under unchanged basic parameters, the reaction at the front end of the CL has reached equilibrium when the gas flow rate reaches 20 mL/min. In summary, the enlarged electrode's capability to accommodate higher gas flows can potentially lead to a reduction in the minimum CL thickness required for optimal performance.

Initially a small sized electrode area of 1.95 cm² was selected to study the flow rate influence, but the effect was minor. Then we explored the impact of the varied flow rate towards performance with different electrode areas. 6 different electrode areas exhibiting a gradient increase and 12 diverse flow rates were systematically chosen for this investigation.

The gradient flow rate impacts largely on the CO₂ molar concentration with different electrode areas, as shown in Fig. 4. To ensure the necessary molar concentration of CO₂ along the CL, each electrode area must satisfy the minimum flow rate necessary to meet the reaction's demands. For example, an electrode area of 20 cm² needs a maximum flow rate of

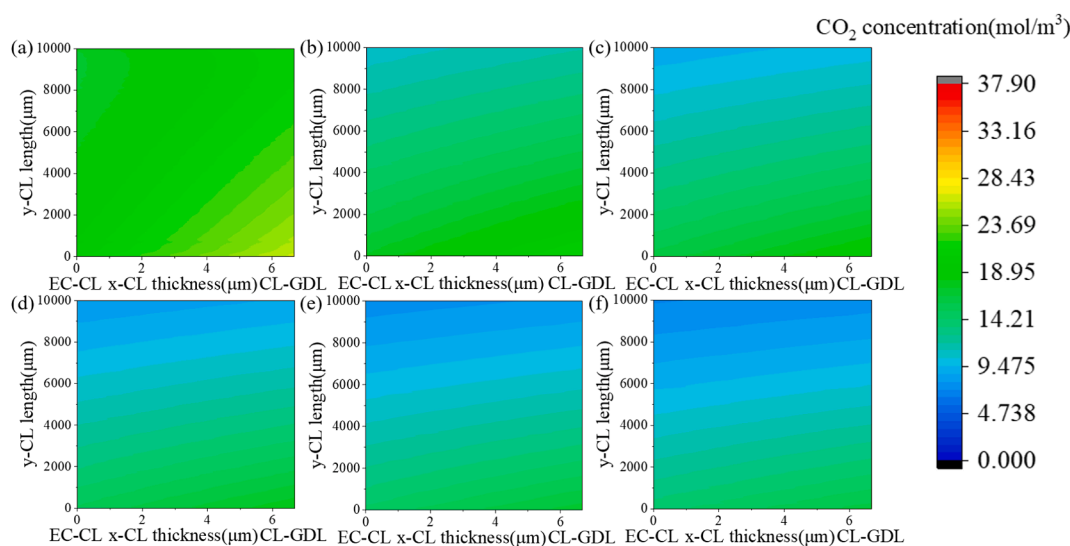


Fig. 2. Under various electrode areas, the distribution of CO₂ concentration at the internal front end of the CL in the same region (y-CL = 10000 μm). Electrode area: (a) 1 cm²; (b) 20 cm²; (c) 40 cm²; (d) 60 cm²; (e) 80 cm²; (f) 100 cm².

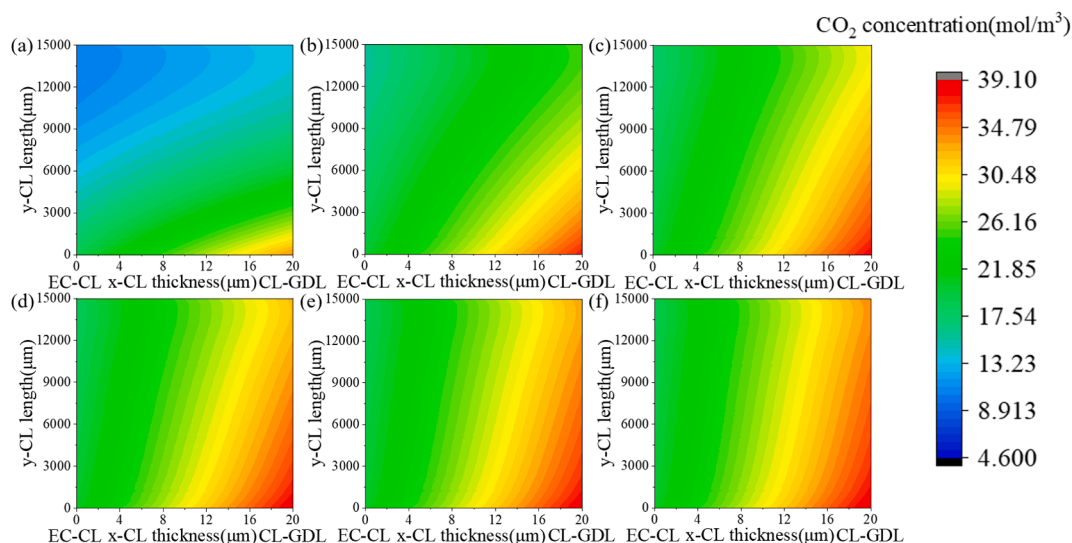


Fig. 3. Distribution of CO_2 concentration within the CL under different gas flow rates. The various gas flow rates are as follows: (a) 1 mL/min; (b) 20 mL/min; (c) 40 mL/min; (d) 60 mL/min; (e) 80 mL/min; (f) 100 mL/min.

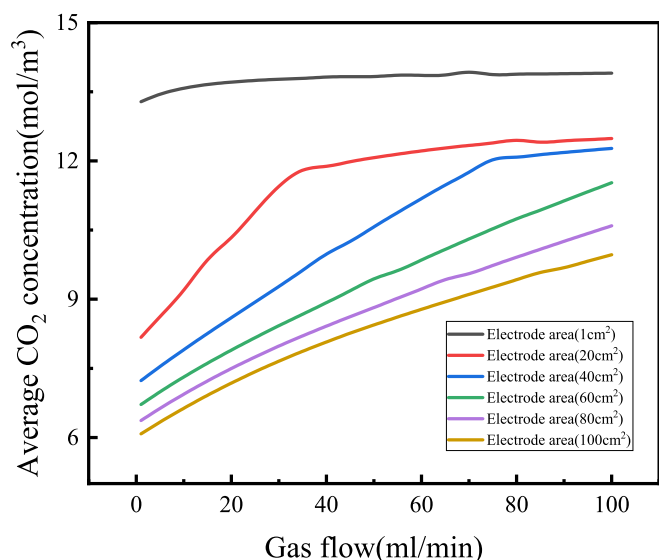


Fig. 4. Average CO_2 concentration distribution in the CL for electrode areas of 1, 20, 40, 60, 80 and 100 cm^2 corresponding to gas flow rates from 0 to 100 mL/min.

approximately 35 mL/min. Beyond this point, exceeding 35 mL/min leads to negligible alterations in the average concentration within the CL, signifying the attainment of the upper consumption limit. However, with the expansion of the electrode area, the flow rate exhibits a gradual increase, reaching up to 100 mL/min (Refer to Table S3 for detailed data). Although the slope of the curve remains nonzero, the concentration on the frontal side remains above zero, indicating an inadequate supply of CO_2 . Considering the accuracy of the COMSOL modelling, along with gas recycling and recovery considerations, we have selected 100 mL/min as the maximum flow rate for larger electrode areas.

The thickness of the CL was chosen as one of the variables. Fig. S5 shows the CO_2 concentration distribution of the CL, and since the CO_2 molar concentration at the back of the electrode remains almost unchanged, the average concentrations of the front, middle and back parts were analysed separately (Fig. S6). The results indicate that when the catalyst thickness reaches 25 μm , its capacity to store CO_2 at the rear reaches its maximum. Under the constraint of limited CO_2 availability,

as the thickness increases, the CO_2 at the front end is continually consumed.

The specific gradient design is shown in Fig. 5(a–f), because the reaction in the CL reaches equilibrium, it is necessary to ensure that its thickness reaches at least 9 μm , this solves the problem that EC-CL does not produce a large number of bubbles that block the catalyst particles. We analysed the molar concentration at the thickness of the CL into 5, 15, 25, 35, 45 and 55 μm , this is to explore the optimal thickness. Fig. 5(a) shows a very high CO_2 molar concentration within the CL, due to the thick is only 5 μm that is too thin for our analysis. Gas entering from the CL-GDL interface undergoes diffusion in the direction across and along the channel, and the rate of this diffusion is strongly correlated with the gas flow rate. We controlled the gas flow rate to be constant and diffused from the gas chamber into the CL at a flow rate of 15 mL/min. Due to the thin thickness of the catalytic layer, the flow rate of the gas is greater than its own diffusion rate, so a gradient concentration change along the channel direction is produced, as shown in Fig. 5(a).

The overall concentration of the CL decreases significantly with increasing thickness ($>9 \mu\text{m}$), indicating ongoing CO_2 consumption at the front end. Increasing the CL thickness changes the gas diffusion rate, with the slope of the gas diffusion concentration distribution tending to increase from 0° , as seen in Fig. 5(b)(c). In Fig. 5(d–f), the molar concentration of CO_2 at the EC-CL interface gradually approaches 0 mol/m^3 as the thickness increases beyond 25 μm . This change ensures maximum CO_2 supply at the rear and shifts the slope of the gas diffusion concentration distribution from 0° to 90° at the EC-CL side, gradually achieving uniform diffusion across the channel. Two primary reasons contribute to this phenomenon: firstly, the increased thickness creates a longer mass transfer distance for CO_2 diffusion from rear to front, reducing the impact of CO_2 mass transfer; secondly, the increased thickness provides a larger effective reaction area, promoting more complete CO_2 consumption.

As the porosity of the GDL changes, the diffusion rate of gas increases within the diffusion layer when porosity is increased. This enhanced diffusion rate facilitates a greater number of CO_2 molecules coming into contact with the catalyst surface, thereby accelerating the reaction rate [40]. On the other hand, an interesting phenomenon is observed, whereby the gas concentration within the catalyst CL remains nearly constant for different porosities, as shown in Fig. S7. Based on the experiments and related simulations by Sinha and colleagues [41], it was shown that Darcy's law, which has a linear relationship between the pressure gradient and flow rate at low flow rates, may be invalid.

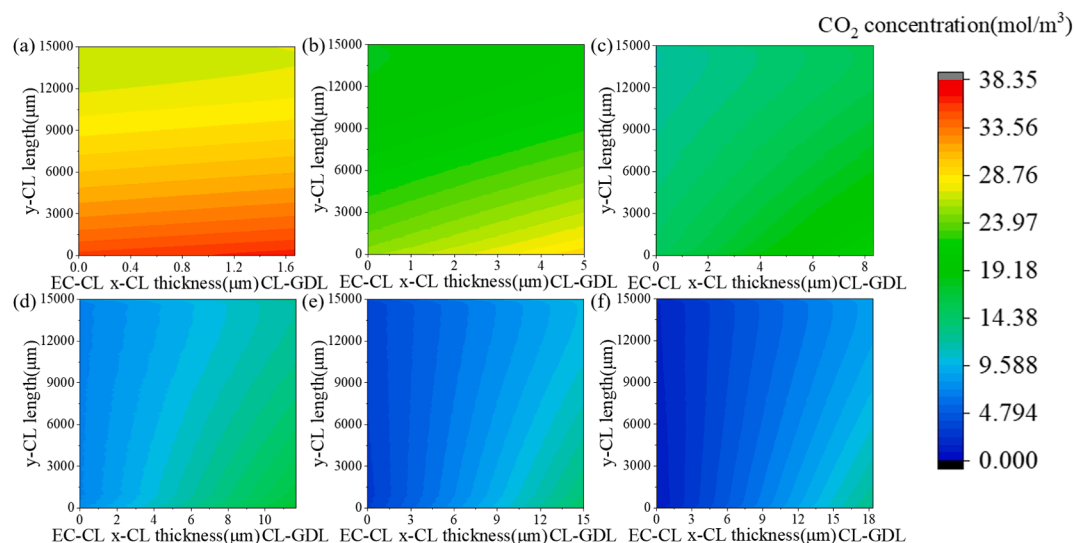


Fig. 5. Distribution of CO₂ concentration at the internal front end of the CL under various CL thicknesses. CL thickness: (a) 5 μm; (b) 15 μm; (c) 25 μm; (d) 35 μm; (e) 45 μm; (f) 55 μm.

When four individual variables are simultaneously varied from six gradients for each variable, the CO₂ molar concentration results are illustrated in Fig. 6 (Refer to Table S4 for detailed data). It is evident that a sole modification in electrode area and CL thickness has a substantial impact on enlargement. In contrast, variations in the GDL porosity and gas flow rate exclusively facilitate enlargement in Case 1 and Case 2.

3.2. Multivariate analysis

We initiated the process by filtering a dataset consisting of 8000 valid nodes. We employed a fixed step size within an established parameter range for this purpose. Subsequently, we utilised LHS method to select 800 nodes for further analysis. These nodes were then applied within the COMSOL model, with CO₂ concentration as the output variable (Refer to Table S5 for detailed data).

The dataset underwent normalisation and was then input into three distinct ML algorithms: RNN-LSTM, RF, and SVM. The process of machine learning algorithms is aided by PythonCharm. The ratio of training

to testing data was set at 8:2, encompassing a total of 30 degrees of freedom. This deliberate choice aimed to enhance the model's stochasticity while mitigating potential concerns related to overfitting. As well as hyper-parameter tuning of different algorithms to better adapt the algorithms to a particular dataset or problem and to improve their performance in terms of prediction accuracy and generalisation ability (Tables S6–S8).

To ensure the reliability of the results and minimize the impact of chance, we conducted cross-validation for the RNN and SVM algorithms. Given that the RF algorithm is inherently capable of avoiding overfitting issues, we employed a randomized validation approach. We executed ten rounds of repeated operations for each algorithm. Subsequently, the results were aggregated to compute both the average CO₂ concentration and the root mean square error coefficient (Figs. S8–S10).

The accuracy rates of 95.79 % for RNN, 98.67 % for RF, and 86.24 % for SVM algorithms are shown in Fig. 7, respectively detailed calculation data is listed in Table S9. The RF algorithm has good stability, which remains at 98.6 ± 0.2 %, with small fluctuations. On the contrary, although the magnitude of parameter differences in RNN is also small, the prediction results are 3 % lower compared to RF algorithm, on the other hand, its prediction accuracy is lower than that of RF algorithm, so we did not use it for modelling. The SVM algorithm has a large

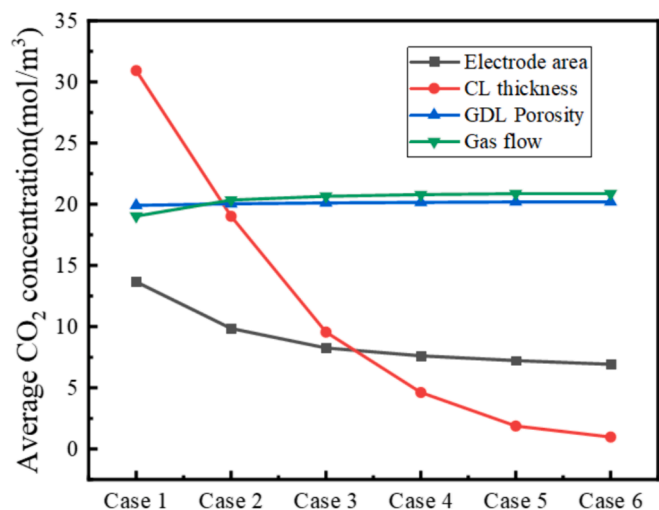


Fig. 6. Single variable & mean concentration at the front end of the CL (Case: grouped gradient), which includes electrode area (1 cm²; 20 cm²; 40 cm²; 60 cm²; 80 cm²; 100 cm²), CL thickness (5 μm; 15 μm; 25 μm; 35 μm; 45 μm; 55 μm.), GDL porosity (0.4; 0.5; 0.6; 0.7; 0.8; 0.9), and gas flow (1 mL/min; 20 mL/min; 40 mL/min; 60 mL/min; 80 mL/min; 100 mL/min.).

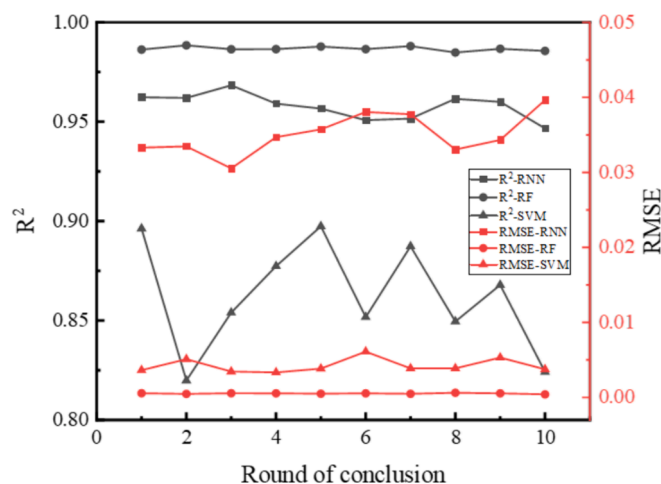


Fig. 7. R² and RMSE based on the three algorithms RNN, RF and SVM.

magnitude of fluctuation, and the difference between the maximum and minimum values is as high as 8 %, and the deviation of its data from the results of multiple calculations is too large, and the magnitude of fluctuation is much larger than that of RNN and RF algorithms. However, R^2 is not the only criterion for evaluation, and the RMSE of the three different algorithms is also evaluated, and the evaluation shows that the RMSE of the three algorithms is less than 0.05, indicating that the prediction results of these three algorithms have small errors, but the error results of RNN, RF and SVM algorithms are 0.0351, 0.0006 and 0.0038 (Table S9). The advantage of RF over the other two algorithms is not only in the higher accuracy, but also in the small error value. The MAE and MAPE are also considered for a more comprehensive evaluation of the algorithm results, and it is also verified that the RF algorithm has a higher degree of fit with the physical model (Table S10). Feature importance analysis is important for the validation of machine learning data, it helps to analyse and understand the degree of influence of different features in the dataset on the target variables, and to analyse the weights of key and secondary variables. Fig. S11 displays the importance of the four variable factors obtained for CO₂ concentration. It found that the thickness, electrode area and gas flow rate had significant impact to the results in the model, but the impact from porosity can be neglected. The feature importance results agree well with simulation results of the single variable, demonstrating that the algorithm performs well. In addition, substituting the data with ML inverse prediction into the original model, comparing the prediction and simulation results of the data-driven surrogate model, and the relative error is 0.32 (as shown in Table S11), indicating a strong correlation between modelling and simulation.

The CO₂ molar concentration along the CL of Case I-IV in relation to the four individual variables: electrode area, CL thickness, GDL porosity, and gas flow, is shown in Fig. 8(a). While maintaining the baseline parameters, the specific values for these individual variable parameters corresponding to each optimal outcome are as follows: electrode area: 1 cm², CL: 55 μm, gas porosity: 0.8, gas flow: 20 mL/min (detailed datasets can be found in Table S12). Notably, the concentration distribution of CO₂ within the CL in Case II is significantly lower when compared to Case I, Case III, and Case IV. This suggests that alterations in the the CL thickness, as a single variable, exert a more substantial influence on the CO₂ conversion within the entire device. In contrast, Case V, incorporating multiple variables, exhibits a lower average CO₂ concentration compared to the scenario with a single variable. The electrode area and the thickness of the catalytic layer play a decisive role in determining the overall concentration, and the variation of these two parameters leads to a larger reaction space for the incoming CO₂, which increases the active area of the reaction, and the sufficient consumption is based on the prerequisite of a guaranteed supply of CO₂ to prevent the error of too low a concentration of CO₂, whereas the size of the porosity directly

determines the mass transfer path of the CO₂ to the surface of the reaction. The case with multiple variables V takes into account the interactions between the above four parameters to show a superior average CO₂ concentration compared to the case with a single variable.

When employing multiple variables, Fig. 8(b) shows the lowest CO₂ molar concentration distribution within the CL (please see Table S13 for details regarding the optimal parameters for the 5 groups). This approach maintains an average CO₂ concentration difference of approximately 1 mol/m³ for the scaling-up process, which falls well within the acceptable range. It's worth mentioning that although A1 yields the lowest average CO₂ molar concentration, an electrode area of 1 cm² is much inadequate for industrial production.

The next step is to find the optimal parameter combinations for A1, A37, A55, A73 and A100 where were predicted using the RF algorithm we developed with the detailed parameter combinations shown in Table S13. Substituting the parameters into the physical model for calculation, yielded the conversion efficiencies of 97.6 %, 96.1 %, 96.2 %, 96.0 % and 97.7 % for the five combinations. Results show the accuracy can be maintained at 96.7 ± 0.94 %, indicating that the prediction result for large sized reactor is meaningful. Meanwhile, in the electrode enlargement study, the gas flow rate should be increased from 19 mL/min to 91 mL/min when the electrode area is expended from 1 to 100 cm². The thickness of the CL is chosen to ensure the maximum value of 73 μm that can be achieved under the accuracy of the physical model, and the porosity is chosen to be 0.8, so that such combinations of variations can keep a high conversion throughout the enlargement process.

4. Conclusion

The effect of four key variables, namely electrode area, CL thickness, GDL porosity, and gas flow, towards CO₂ molar concentration along the CL in both longitudinal and transverse dimensions are studied in both single variable and combined multiple variable models. RF ML algorithm was used as the most suitable method for developing a 2D COMSOL Multiphysics model for scale-up investigation. Low CO₂ molar concentration within an enlarged electrode area was not solely responsible for a complete reactant consumption; it was also related to CO₂ supply insufficiency due to the bigger electrode area's size, longitudinal diffusion, and insufficient gas flow. The CL's thickness was found to have a significant impact on CO₂ amount and bubble generation at the EC-CL interface, with optimal thickness identified as 73 μm. The influence of GDL porosity was less important due to a trade-off between gas quantity and equilibrium concentration. Simultaneously considering these four variables, LHS was applied for data collection and selection, and the RF showed excellent results of R^2 and RMSE values of 98.67 %, and 0.0006, respectively. This data-driven model met experimental requirements while significantly reducing computational time and costs

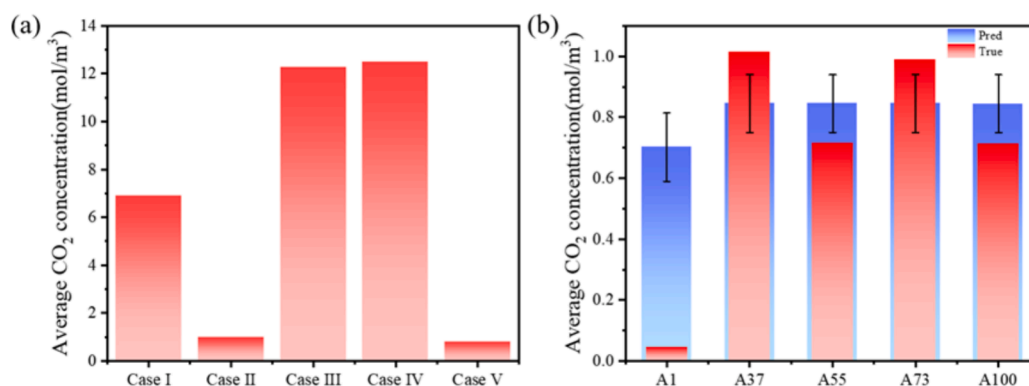


Fig. 8. (a) Cases I-IV: single-variable minimum average concentration values (electrode area, CL thickness, GDL porosity, gas flow rate); Case V: multivariate combination of AI-calculated minimum average concentration values; (b) Comparison of predicted and true multivariate minimum average concentration values for electrode areas of 1, 37, 55, 73, and 100 cm².

for scaling up. We applied this model to a 100 cm² electrode area reactor and received result of high and consistent CO₂ conversion efficiency of 96.7 ± 0.94 %, at a GDL porosity of 0.8 and a flow rate of 91 mL/min.

CRedit authorship contribution statement

Guyu Zhang: Writing – original draft, Methodology, Investigation, Data curation, Conceptualization. **Xiaoteng Liu:** Writing – review & editing, Supervision, Funding acquisition, Conceptualization. **Hanhui Lei:** Writing – review & editing, Formal analysis, Conceptualization. **Yucheng Wang:** Validation, Resources, Data curation. **Denise Bildan:** Writing – review & editing, Visualization. **Xiangqun Zhuge:** Writing – review & editing, Supervision. **Lei Xing:** Writing – review & editing, Formal analysis, Conceptualization. **Kun Luo:** Writing – review & editing, Supervision.

Declaration of competing interest

The authors declare that they have no known competing financial interests or personal relationships that could have appeared to influence the work reported in this paper.

Data availability

Data will be made available on request.

Acknowledgements

The authors gratefully acknowledge the financial support from the Jiangsu Specially-Appointed Professor Fund by Jiangsu Education Department, Science and Technology Plan Project of Changzhou (No. CQ20D2EHPA034), the UK Engineering Physics and Science Research Council (Grant No. EP/S032886/1).

Appendix A. Supplementary material

Supplementary data to this article can be found online at <https://doi.org/10.1016/j.fuel.2024.132400>.

References

- [1] Sullivan I, Goryachev A, Digdaya IA, Li XQ, Atwater HA, Vermaas DA, et al. Coupling electrochemical CO₂ conversion with CO₂ capture. *Nat Catal* 2021;4(11):952–8.
- [2] Senocrate A, Battaglia C. Electrochemical CO₂ reduction at room temperature: status and perspectives. *J Energy Storage* 2021;36:7.
- [3] Jin S, Hao ZM, Zhang K, Yan ZH, Chen J. Advances and challenges for the electrochemical reduction of CO₂ to CO: from fundamentals to industrialization. *Angew Chem-Int Edit* 2021;60(38):20627–48.
- [4] Fernández-Caso K, Díaz-Sainz G, Alvarez-Guerra M, Irabien A. Electroreduction of CO₂ advances in the continuous production of formic acid and formate. *ACS Energy Lett* 2023;8(4):1992–2024.
- [5] Lu S, Wang YC, Xiang H, Lei HH, Xu BB, Xing L, et al. Mass transfer effect to electrochemical reduction of CO₂: electrode, electrocatalyst and electrolyte. *J Energy Storage* 2022;52:20.
- [6] Gao D, Wei P, Li H, Lin L. Designing electrolyzers for electrocatalytic CO₂ reduction. *Acta Phys-Chim Sin* 2020;37:2009021.
- [7] Marcandalli G, Monteiro MCO, Goyal A, Koper MTM. Electrolyte effects on CO. *Acc Chem Res* 2022;55(14):1900–11.
- [8] Albo J, Perfecto-Irigaray M, Beobide G, Irabien A. Cu/Bi metal-organic framework-based systems for an enhanced electrochemical transformation of CO₂ to alcohols. *J CO₂ Utiliz* 2019;33.
- [9] Albo J, Sáez A, Solla-Gullón J, Montiel V, Irabien A. Production of methanol from CO₂ electroreduction at Cu₂O and Cu₂O/ZnO-based electrodes in aqueous solution. Production of methanol from CO₂ electroreduction at Cu₂O and Cu₂O/ZnO-based electrodes in aqueous solution. *Appl Catal B: Environ* 2015.
- [10] Goyal A, Marcandalli G, Mints VA, Koper MTM. Competition between CO₂ reduction and hydrogen evolution on a gold electrode under well-defined mass transport conditions. *J Am Chem Soc* 2020;142(9):4154–61.
- [11] Yoo JS, Christensen R, Vegge T, Norskov JK, Studt F. Theoretical insight into the trends that guide the electrochemical reduction of carbon dioxide to formic acid. *ChemSusChem* 2016;9(4):358–63.
- [12] Dodds WS, Stutzman LF, Sollami BJ. Carbon dioxide solubility in water. *Ind Eng Chem Chem Eng Data* 1956;1(1):92–5.
- [13] Dinh CT, Burdyny T, Kibria MG, Seifitokaldani A, Gabardo CM, de Arquer FPG, et al. CO₂ electroreduction to ethylene via hydroxide-mediated copper catalysis at an abrupt interface. *Science* 2018;360(6390):783–7.
- [14] de Arquer FPG, Dinh CT, Ozden A, Wicks J, McCallum C, Kirmani AR, et al. CO₂ electrolysis to multicarbon products at activities greater than 1 A cm⁻². *Science* 2020;367(6478):661.
- [15] Albo J, Vallejo D, Beobide G, Castillo O, Castao P, Irabien AJC. Copper-based metal-organic porous materials for CO₂ electrocatalytic reduction to alcohols. *ChemSusChem* 2017;10.
- [16] Wang YC, Lei HH, Xiang H, Fu YQ, Xu CX, Jiang YZ, et al. Porous bilayer electrode guided gas diffusion for enhanced CO₂ electrochemical reduction. *Adv Energy Sustain Res* 2021.
- [17] Albo J, Irabien A. Cu₂O-loaded gas diffusion electrodes for the continuous electrochemical reduction of CO₂ to methanol. *J Catal* 2016.
- [18] Xing Z, Hu L, Ripatti DS, Hu X, Feng XF. Enhancing carbon dioxide gas-diffusion electrolysis by creating a hydrophobic catalyst microenvironment. *Nat Commun* 2021;12(1):11.
- [19] Wang YC, Lei HH, Lu S, Yang ZM, Xu BB, Xing L, et al. Cu₂O nano-flowers/graphene enabled scaffolding structure catalyst layer for enhanced CO₂ electrochemical reduction. *Appl Catal B-Environ* 2022;305:10.
- [20] Merino-García I, Albo J, Irabien A. Tailoring gas-phase CO₂ electroreduction selectivity to hydrocarbons at Cu nanoparticles. *Nanotechnology* 2019.
- [21] Merino-García I, Tinat L, Albo J, Alvarez-Guerra M, Irabien A, Durupthy O, et al. Continuous electroconversion of CO₂ into formate using 2nm tin oxide nanoparticles. *Appl Catal B: Environ* 2021;297:120447.
- [22] Merino-García I, Albo J, Solla-Gullón J, Montiel V, Irabien A. Cu oxide/ZnO-based surfaces for a selective ethylene production from gas-phase CO₂ electroconversion. *J CO₂ Utiliz* 2019;31:135–42.
- [23] Oh S, Park H, Kim H, Park YS, Ha MG, Jang JH, et al. Fabrication of large area Ag gas diffusion electrode via electrodeposition for electrochemical CO₂ reduction. *Coatings* 2020;10(4):14.
- [24] Li J, Chen G, Zhu Y, Liang Z, Cui Y. Efficient electrocatalytic CO₂ reduction on a three-phase interface. *Nat Catal* 2019.
- [25] Lei HH, Xing L, Jiang H, Wang YC, Bin Xu B, Xuan J, et al. Designing graded fuel cell electrodes for proton exchange membrane (PEM) fuel cells with recurrent neural network (RNN) approaches. *Chem Eng Sci* 2023;267:14.
- [26] Gao Y, Montana A, Chen FX. Evaluation of porosity and thickness on effective diffusivity in gas diffusion layer. *J Power Sources* 2017;342:252–65.
- [27] He RA, Xu NN, Ul Hasan IM, Peng LW, Li LL, Huang HT, et al. Advances in electrolyzer design and development for electrochemical CO₂ reduction. *EcoMat* 2023;5(7):17.
- [28] Burdyny T, Smith WA. CO₂ reduction on gas-diffusion electrodes and why catalytic performance must be assessed at commercially-relevant conditions. *Energy Environ Sci* 2019;12(5):1442–53.
- [29] Kas R, Yang K, Bohra D, Kortlever R, Burdyny T, Smith WA. Electrochemical CO₂ reduction on nanostructured metal electrodes: fact or defect? *Chem Sci* 2020;11(7):1738–49.
- [30] Kotb Y, Fateen SEK, Albo J, Ismail I. Modeling of a microfluidic electrochemical cell for the electro-reduction of CO₂ to CH₃OH. *Electrochem Soc* 2017;13.
- [31] Kas R, Star AG, Yang KL, Van Cleve T, Neyerlin KC, Smith WA. Along the channel gradients impact on the spatioactivity of gas diffusion electrodes at high conversions during CO₂ electroreduction. *ACS Sustain Chem Eng* 2021;9(3):1286–96.
- [32] Altman N, Krzywinski M. Points of significance: ensemble methods: bagging and random forests. *Nat Methods* 2017;14(10):933–4.
- [33] Hearst MA, Dumais ST, Osuna E, Platt J, Scholkopf B. Support vector machines. *IEEE Intell Syst* 1998;13(4):18–28.
- [34] Zheng L, Hou Y, Zhang T, Pan X. Performance prediction of fuel cells using long short-term memory recurrent neural network. *Int J Energy Res* 2021;45(6):9141–61.
- [35] Han IS, Chung CB. Performance prediction and analysis of a PEM fuel cell operating on pure oxygen using data-driven models: a comparison of artificial neural network and support vector machine. *Int J Hydrogen Energ* 2016;41(24):10202–11.
- [36] Huo W, Li W, Zhang Z, Sun C, Zhou F, Gong G, et al. Performance prediction of proton-exchange membrane fuel cell based on convolutional neural network and random forest feature selection. *Energy Conversion* 2021;243:114367.
- [37] Wu KN, Birgersson E, Kim B, Kenis PJA, Karimi IAJJ. Modeling and experimental validation of electrochemical reduction of CO₂ to CO in a microfluidic. *Cell* 2015;162(1):F23–32.
- [38] Yang ZM, Li D, Xing L, Xiang H, Xuan J, Cheng SA, et al. Modeling and upscaling analysis of gas diffusion electrode-based electrochemical carbon dioxide reduction systems. *ACS Sustain Chem Eng* 2021;9(1):351–61.
- [39] Wu J, Sharma PP, Harris BH, Zhou XD. Electrochemical reduction of carbon dioxide: IV dependence of the Faradaic efficiency and current density on the microstructure and thickness of tin electrode. *J Power Sources* 2014;258:189–94.
- [40] Xing L, Wang Y, Das PK, Scott K, Shi WD. Homogenization of current density of PEM fuel cells by in-plane graded distributions of platinum loading and GDL porosity. *Chem Eng Sci* 2018;192:699–713.
- [41] Sinha S, Hansen A. Effective rheology of immiscible two-phase flow in porous media. *EPL* 2012;99(4):6.